Learning and Nonlinear Models - Journal of the Brazilian Society on Computational Intelligence (SBIC), Vol. 23, Iss. 1, pp. 19–32, 2025
https://doi.org/10.21528/lnlm-vol23-no1-art2

SYMMETRY FEATURE ESTIMATION OVER STFT TRANSFORM TO IMPROVE RADAR CLASSIFICATION BASED ON THE WISARD WEIGHTLESS NEURAL NETWORK

Rodrigo Moreira, Jorge Pires and Aline de Oliveira
Instituto de Pesquisas da Marinha
{silva.moreira,aline.oliveira,jorge.costa}@marinha.mil.br

Abstract – Automated early recognition of enemy radar emissions are essential for the survival of a warship. Radar signals intercepted by a passive digital Electronic Support Measure (ESM) receiver can be classified based on the type of intrapulse modulation. The modulation classification is typically based on features extracted from the preprocessed radar's signal. Low Probability of Intercept (LPI) radars can use phase or frequency modulated signals to make radar emissions difficult for the enemy to detect. This paper proposes the use of a new feature, the symmetry measured in a Time-Frequency (TF) matrix, to improve intrapulse radar modulation classification. The analysis of the symmetry in a STFT matrix is characterized by an image processing problem, where the matrix is interpreted as a grayscale image. This paper also proposes the use of Weightless Neural Network WiSARD in identifying symmetry patterns in the Short Time Fourier Transform (STFT) matrix, a characteristic present in signals with Barker and Polytime phase modulations and which can be used by classifiers to discriminate them from signals with other types of modulations such as polyphase modulations (P1, P2, P3, P4 and Frank), linear frequency modulation (LFM), and Non Linear Frequency Modulation.

Keywords – WiSARD, classification, artificial intelligence, feature, time-frequency transform.

1. INTRODUCTION

When it comes to radar signal classification in ESM equipment, real-time processing is highly crucial to minimize response time and achieve adequate crew reaction time against a threat. This is crucial for the survival of the platform where ESM receiver is installed. The ESM system needs to quickly identify specific modulations of radar emitters, such as LPI intrapulse phase modulation and frequency modulation, communicating to the defense system a nearby and likely threat.

The WiSARD is a computing tool that was initially designed to classify images [1]. It is a weightless neural network composed of some discriminators that decides the class of an input data doing only one arithmetic operation, the sum, and comparing the sum results. It has a very fast training [2–4], which is a very important feature that usually causes WiSARD to be chosen even if other classifieres have a closer but better accuracy. The fast test time is another important feature [5], because the memory access and the sum operation can be done in a short period of time. This feature makes it possible to use the WiSARD network for real-time applications, such as in ESM equipments. The WiSARD can easily be implemented in a GPU [6] and in a FPGA [7].

There are many papers about classification of radar signal modulation in literature. It is a widely studied problem, with many proposed solutions. The use of a Time-Frequency transform to detect a signal and estimate features used in training a classifier is explored in several works. Many authors apply a TF transform [8–14] to phase-modulated signals or a similar transform [15–17] to analyze them from a different perspective. It's noticeable that the results obtained from transforms applied to signals of each modulation type can highlight some of their particular characteristics, making the classification problem easier to solve. Some authors classify phase-modulated signals using the Choi-Williams Distribution (CWD) [8,9,11,12,14] or the modified CWD [13] due to their immunity to noise, while others prefer using the STFT [10] because of its processing time. Kishore [18] proposed increasing the Signal-to-Noise ratio (SNR) through the use of the Wigner Ville Distribution (WVD) transform, which employs instantaneous autocorrelation function as its kernel. The reduction in noise presence occurs as it becomes uncorrelated. Some works address classification in a spectral domain where it's possible not only to classify signals with noise immunity but also to more efficiently estimate other important signal characteristics like bandwidth and central frequency [15–17]. CNN [8,10,12–14], SVM [11,16], Decision Tree [18], and SSD [9] are some examples of classifiers used to identify phase modulation type based on the TF transform result. The Weightless Neural Network WiSARD can also be utilized for this purpose (Fig. 1). First the signal samples are transformed by a TF transform. The result matrix is binarized using an image processing algorithm of binarization. The new matrix of binary numbers can be used as images to train the WiSARD discriminators responsible for generating the final classification.

This paper proposes the use of a new feature, the symmetry, estimated in the TF matrix, to improve intrapulse radar modulation classification. This approach can be quickly extracted with a WiSARD weightless neural network [1]. We will show that the symmetry feature increases the classification accuracy of LPI radar signals. This approach can be used by classifiers to better separate the Barker [19] and Polytime [20] phase-modulated signals, that have TF symmetry, from other types of phase and

https://doi.org/10.21528/lnlm-vol23-no1-art2

frequency-modulated radar signals, such as Frank [21], P1 [22], P2 [22], P3 [23], P4 [23], and LFM [24], which do not have TF symmetry.

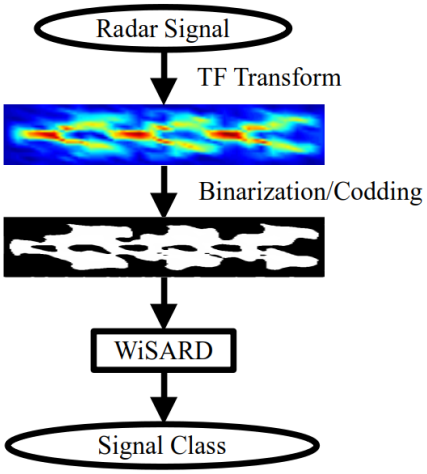

Figure 1: The WiSARD neural network designed to classify radar-signal modulations.

2. CLASSIFICATION OF INTRAPULSE MODULATION

Identifying the type of intrapulse modulation (MOP) can be crucial in determining whether a radar signal poses a threat. The classification also provides valuable information about the electromagnetic environment, helping to better understand the presence of different types of signals, their origin and behavior. After classifying a MOP signal as hostile, the combat system can react, keeping safe the platform where ESM receiver is installed.

Radar intrapulse modulation has a lot of applications. Tracking radars can determine more precisely the target position and velocity through the pulse compression technique. In this way, the radar transmits phased modulated pulses where pulses' echoes will be processed by its matched filters to produce a pulse with lower pulse width. Using compressed pulses, a surveillance system can detect with more accuracy the quantity of enemy aircrafts in a squadron. Navigation radars can use intrapulse compression to improve their navigation precision when necessary. The matching filter also provides a SNR gain, so longer ranges can be achieved with the same transmission power. LPI radars, a kind of radar that camouflages itself by reducing signal transmission power, can use the intrapulse compression to reduce the transmission power without loosing the range of detection, although it is more common to use a frequency modulated continuous wave instead of pulsed wave for LPI transmissions or, less commonly, a phase modulated continuous wave [25]. Low Probability of Identification (LPID) radars, which have the characteristic of making identification difficult, can use for this purpose the transmission of random phased modulated pulses.

The first process that occur in a ESM equipment is the detection of a radar signal, $s(t)$, with a carrier frequency, f_c, and pulse width, T. The electromagnetic spectrum is observed by the antenna of the ESM receiver. In the front-end of the ESM receiver, the electrical field of the spectrum is converted to an electrical signal, amplified by a low noise amplifier and downconverted to an intermediary frequency f_i. An analog to digital converter digitalizes the electrical signal and the detection process decides if there exists an radar signal or not [26]. The detected signal can be frequency modulated, phase modulated, or not have any kind of modulation. Furthermore, the detected radar signal is corrupted by noise according to the equation (1) [10].

$$s(t) = A\cos(2\pi f_c t + \varphi(t) + \psi) + n(t), t \in [T_{OA}, T_{OA} + T), \tag{1}$$

where A is the signal amplitude in Volts, f_c is the carrier frequency, $\varphi(t)$ is the intrapulse modulation function, T_{OA} is the time of arrival, the time that the radar signal was detected, ψ is the initial phase and $n(t)$ is a circular complex AWGN process representing the noise.

Basically, the ESM equipment needs to identify two types of MOP: frequency modulation (FMOP) [18, 27] and phase modulation (PMOP) [10, 11, 16, 27, 28]. Each one of these modulations can be expressed by defining the function $\varphi(t)$ (Eq. (1)). A linear frequency modulated pulsed radar signal (LFM) [18, 27, 28], also known as Chirp signal, linearly varies its frequency with respect to time as expressed in Equation (2) [18].

$$\varphi(t) = \pi\alpha t^2, t \in [T_{OA}, T_{OA} + T), \tag{2}$$

where α is the chirp rate, an important feature to be measured by the ESM receiver.

The Barker codes were introduced by Ronald Hugh Barker [19]. As a type of PMOP modulation, the signal phase changes at various instants of time during the pulse transmission. Every phase modulated signal is implemented by dividing the signal pulse into equal time intervals referred to as time segments. In the case of Barker-type modulation [11, 19] and other polyphase

modulations [10, 11, 16, 21, 27, 28] like Frank, P1, P2, P3, and P4, the signal maintains constant the phase within each segment and may change the phase between one segment and the next. On the other hand, the time segment of a polytime modulated signal [10, 11, 16, 20, 27, 28] is not constant, so the time that the signal stays in a specific phase state is variable.

Concerning Barker-type modulation, the signal's phase within each time segment can be 0^o or 180^o, representing the two phase states generated by this modulation technique, whereas in the case polyphase-type modulation, three or more phase states are generated. Equation (3) shows the phase values of a Barker13 modulated signal.

$$\varphi(t) = \begin{cases} 0, t \in [T_{OA}, T_{OA} + \frac{5}{13}T] \bigcup [T_{OA} + \frac{7}{13}T, T_{OA} + \frac{9}{13}T] \bigcup [T_{OA} + \frac{10}{13}T, T_{OA} + \frac{11}{13}T] \bigcup [T_{OA} + \frac{12}{13}T, T] \\ \pi, t \in [T_{OA} + \frac{5}{13}T, T_{OA} + \frac{7}{13}T] \bigcup [T_{OA} + \frac{9}{13}T, T_{OA} + \frac{10}{13}T] \bigcup [T_{OA} + \frac{11}{13}T, T_{OA} + \frac{12}{13}T] \end{cases} \tag{3}$$

The idea of the Barker code is to generate a signal that minimizes the energy of the first sidelobe of the autocorrelation function. T1 and T2 Polytime sequences are derived using a stepped-RF underlying model [20]. T3 and T4 Polytime sequences are approximations to a LFM underlying model [20]. The Frank [21], P1 [22] and P2 [22] polyphase codes derive from a stepwise approximation of an LFM waveform. P3 and P4 polyphase codes are conceptually derived from a linear frequency modulation waveform [23].

Equations (4) to (8) shows the phase value of a Frank, P1, P2, P3 and P4 modulated signal respectively. On the other hand, equations (9) to (12) present the phase value of a T1, T2, T3 and T4 modulated signal, respectively.

$$\varphi(i(t), j(t)) = \frac{2\pi}{M}(i-1)(j-1), t \in [T_{OA}, T_{OA} + T), A = \{x \in \mathbb{N} : 1 \leq x \leq M\}, i \in A, j \in A, \tag{4}$$

where M is the order of the Frank code [16, 18, 21], with each phase based on the $i(t)$ and $j(t)$ values.

$$\varphi(i(t), j(t)) = \frac{-\pi}{L}\left[L - (2j-1)\right]\left[L(j-1) + (i-1))\right], t \in [T_{OA}, T_{OA} + T), B = \{x \in \mathbb{N} : 1 \leq x \leq L\}, i \in B, j \in B \tag{5}$$

$$\varphi(i(t), j(t)) = \frac{-\pi}{2L}(2i - 1 - L)(2j - 1 - L), t \in [T_{OA}, T_{OA} + T), i \in B, j \in B \tag{6}$$

L in Equation (5) and Equation (6) represents the order of P1 and P2 code respectively [16, 18].

$$\varphi(i(t), j(t)) = \frac{\pi}{Q}(i-1)^2, t \in [T_{OA}, T_{OA} + T), C = \{x \in \mathbb{N} : 1 \leq x \leq Q\}, i \in C \tag{7}$$

$$\varphi(i(t), j(t)) = \frac{\pi}{Q}(i-1)^2 - \pi(i-1), t \in [T_{OA}, T_{OA} + T), i \in C \tag{8}$$

Q in Equation (7) and Equation (8) is the compression ratio of the P3 and P4 codes respectively [16, 18].

$$\varphi_t = mod\left\{\frac{2\pi}{N} INT\left[(kt - jT)\frac{jN}{T}, 2\pi\right]\right\}, t \in [T_{OA}, T_{OA} + T), D = \{x \in \mathbb{N} : 0 \leq x \leq k-1\}, j \in D \tag{9}$$

$$\varphi_t = mod\left\{\frac{2\pi}{N} INT\left[(kt - jT)(\frac{2j-k+1}{T})\frac{n}{2}, 2\pi\right]\right\}, t \in [T_{OA}, T_{OA} + T), j \in D \tag{10}$$

In Equation (9) and Equation (10), j is the segment index, k is the number of segments and n is the number of phase states [20].

$$\varphi_t = mod\left\{\frac{2\pi}{N} INT\left[\frac{nBt^2}{2T}, 2\pi\right]\right\}, t \in [T_{OA}, T_{OA} + T) \tag{11}$$

$$\varphi_t = mod\left\{\frac{2\pi}{N} INT\left[\frac{nBt^2}{2T} - \frac{nBt}{2}, 2\pi\right]\right\}, t \in [T_{OA}, T_{OA} + T) \tag{12}$$

In Equation (11) and Equation (12), n is the number of phase states and B is the signal frequency excursion [20].

The goal of a classifier is to predict the correct class of an input data, which can be represented by a set of variables forming the feature vector x_i. In the case of modulation recognition, the classes are the signal modulation types (Eq. (2) to Eq. (12)) and the feature vector is formed calculating features from the digitalized signal samples and from the TF transform result applied to the same samples. In a generic sense, an input data has a single associated label y_i, referred to as its class. The training of a classifier involves seeking a function f (Eq. (13)) that accurately identifies the class of a given input test data.

$$f : x_i \rightarrow y_i \tag{13}$$

The supervised adjustment of function f is carried out using a training set Tr (Eq. (14)).

https://doi.org/10.21528/lnlm-vol23-no1-art2

$$Tr = (x_i, y_i), \{i \in \mathbb{N} : 1 \leq i \leq QT\}, \tag{14}$$

where each element of the training set is the pair (x_i, y_i), x_i is the feature vector representing an input data, y_i is the output which is the associated class for the input data x_i, and QT is the quantity of elements in the training set. Once the function is defined through supervised training of the classifier, it is used to predict the class of each new input data, referred to as a test data. The function f divides the feature space directly or indirectly into regions that are associated with classes. Predicting the class involves determining the region to which the input data x_i belongs.

3. WiSARD WEIGHTLESS NEURAL NETWORK

In the field of neural networks, one of the primary research directions is that of weightless neural networks. In these networks, the inputs and outputs of neurons are binary numbers 0,1, and there are no weights between the neurons. The functions of each neuron are stored in tables that can be implemented in RAM memories. The learning process of artificial neural networks involves adjusting weights. Unlike traditional neural networks, whose learning process amounts to adjusting synaptic weights, the analogous process for weightless models is accomplished by modifying the values stored in tables, allowing the development of flexible algorithms with rapid learning. The fast speed of learning is due to the mutual independence among the nodes when the input data to the network is altered, crucial for the application addressed in this paper. In artificial neural networks, changing the value of weights while it is learning changes how the node behaves relative to the patterns already trained, which does not occur in weightless neural networks. The use of tables enables the implementation of any function in the nodes since any binary value can be stored in response to a set of input bits during training.

The weightless neural network WiSARD was created by Wilkes, Stonham, and Aleksander in 1984 [1]. WiSARD is a neural network applicable to classification, regression, pattern detection, and other problems. [29] introduced KernelCanvas, a method generating fixed-size binary codes derived from spatiotemporal patterns, suitable for WiSARD networks. The combined approach of KernelCanvas with WiSARD classifier was compared against various established classifiers across four classification tasks: human movements, handwritten characters, speaker recognition, and speech recognition. In these comparisons, WiSARD occasionally yielded inferior results only to the considerably slower K-Nearest Neighbors approach. Moreover, WiSARD demonstrated strong classification performance in diverse applications such as early epileptic seizure detection [2], astronomical object classification in the Galaxy M81 [30], identification of biases in news articles [3], detection of road pavement defects [31], social network text categorization [5], preclinical marker classification in Alzheimer's disease [32], facial expression recognition [33], and maritime vessel tracking [6].

Massimo [4] extensively tested WiSARD across numerous problem domains and compared its performance with state-of-the-art classifiers, consistently concluding that WiSARD exhibits similar performance to the best ones. Furthermore, WiSARD demonstrates suitability for rapid implementation in Field Programmable Gate Arrays (FPGA) [7] and Graphics Processing Units (GPU) [6].

The WiSARD neural network comprises a set of fundamental components known as discriminators. Each discriminator is responsible for recognizing distinct classes of patterns. These discriminators consist of nodes that store 1-bit words 0,1 and can be implemented using Random Access Memory. The output of each discriminator is the sum of its nodes' outputs (Fig. 2). Therefore, in a classification problem, when an input is given to the WiSARD network, the discriminator that yields the highest sum determines the class of the input data.

The training of the network, in the classification problem, is conducted on a per-discriminator basis. In the context of recognizing intrapulse modulation of radar signals, one of the classes to be identified might represent phase-modulated pulsed signals by Barker sequences. In this scenario, one of the discriminators is trained exclusively with signals from this particular class. The same is done with the other classes. Initially, before start the training, all addresses of all nodes within the network are set to store the value 0. During the training phase, a binary image (Fig. 2), derived from the binarization of the response of a Barker pulse to the Short-Time Fourier Transform (STFT), is fed into the discriminator representing the Barker class. This is repeated until the last Barker test signal. Each address of the RAM memories of this discriminator that is accessed, is set to store the value 1 [6]. Consequently, during the network's testing phase, whenever an image resulting from the binarization of the STFT-applied Barker pulse is presented, it is more likely that a greater number of nodes within the discriminator representing the Barker class will return the value 1, while nodes within discriminators representing other classes will likely return 0. Following the summation across each discriminator, it is more probable that the highest response (the sum of its nodes) will originate from the discriminator representing the Barker class. Therefore, the WiSARD network will decide in favor of the Barker class.

The number of points in the image connected to each node within a discriminator is identical and chosen randomly (Fig. 2). The random connections of all nodes to the image within a discriminator are termed as the input mapping. Once the input mapping is set, it remains unchanged throughout both the training and classification/test phases.

4. PROPOSED SYMMETRY ESTIMATION

One of the most important tasks in a ESM equipment is to estimate what is the radar signal modulation type. Some kinds of frequency and phase modulations can be identified by the time-frequency analysis. Figure 3 shows the STFT of some radar signals modulated in phase and frequency. It is easy to see that each type of intrapulse modulation produces a different STFT matrix, which can be interpreted as an image, making the classification of the modulation type basically a visual computing

https://doi.org/10.21528/lnlm-vol23-no1-art2

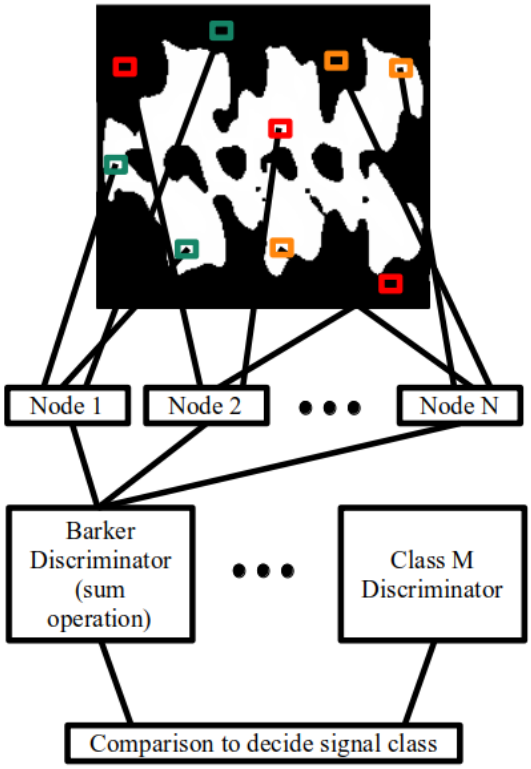

Figure 2: WiSARD neural network .

problem. Tracing an horizontal line in the middle of the images, it becomes clear that the only image that has a certain symmetry in relation to the line due to spectral spread is the Barker 13 phase modulated signal image. In other words, if the symmetry of each image is computed, the Barker 13 image will produce a higher value.

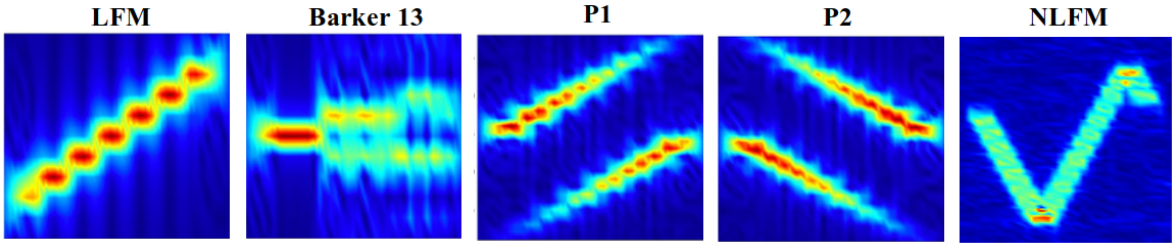

Figure 3: STFT of some radar signals modulated in phase and frequency. The horizontal axis is the time. The vertical axis is the frequency. The red color represents bigger values. Lower values are represented by the blue color.

Figure 4 shows how the symmetry estimation can be done using the WiSARD. After applying the STFT to the input signal, the binarization/coding process starts. The aim of this process block is to transform the STFT result matrix into a binary matrix. The binary matrix is divided equally in two rectangles. The upper rectangle has the bits used to train one discriminator of the WiSARD, the other one has the bits to estimate the image symmetry. Our proposal is to use an input mapping for the symmetry estimation mirrored to the training input mapping (Fig. 5). If the image is symmetrical in relation to the horizontal line, this proposed WiSARD configuration will return a high response, otherwise the return will be a low value.

The biggest challenge of the symmetry estimation is to calculate it accurately even in presence of noise. Figure 6 shows how the STFT response is affected by a low SNR. If the noise power is relevant in relation to the signal power (Fig. 6, right), the measurement tends to be inaccurate because the highest STFT values, which are the most relevant and which should be the values referring to the signal, now refer to the signal and noise. That is one of the reasons why to use a Machine Learning computational tool to estimate the symmetry. The symmetry could be simply measured by the inverse of the template matching calculus such as the Normalized Sum of Absolute Differences (NSAD) [34], the Normalized Cross Correlation [35] and the Normalized Sum of Squared Differences [36]. But the simulations showed that these measurements can fail when the SNR is low (section 5). In addition to enabling very fast training, the WiSARD can be generalized at the node level using GRAM nodes [37] to increase resilience to the presence of noise. The symmetry estimation in STFT images to improve Barker signals classification, the use

https://doi.org/10.21528/lnlm-vol23-no1-art2

of the WiSARD to estimate the symmetry and the use of GRAM to increase the resilience to the noise were the contributions of this paper.

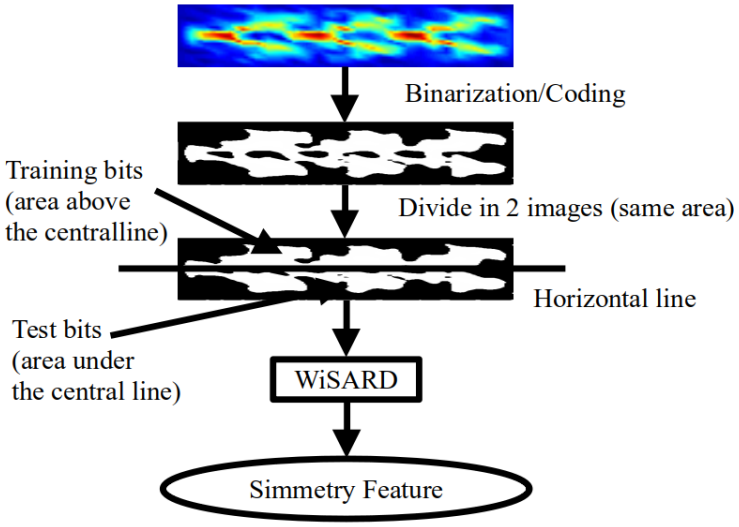

Figure 4: Use of the WiSARD neural network to estimate the symmetry.

5. SIMULATIONS AND RESULTS

The objective of this paper is to demonstrate that classifiers can enhance the accuracy of modulated signal classification by incorporating estimated symmetry in the time-frequency plane into the feature vector x_i. In order to achieve the objectives, simulations were conducted using MATLAB version 2023a.

The analyzed signals include radar pulses simulated with intrapulse modulations such as Linear Frequency Modulation (LFM), Barker13, polyphase modulations (Frank, P1, P2, P3, and P4), and polytime modulations (T1, T2, T3, and T4). Fourteen different Signal-to-Noise ratio (SNR) values were considered for the signals (in dB): [-25, -20, -17.5, -15, -12.5, -10, -7.5, -5, -2.5, 0, 2.5, 5, 10, 15]. A total of 140 signals of each modulation type were used. The considered noise was Additive White Gaussian Noise. The pulse width (PW) of the signals were $10\mu s$.

The objective of the first three simulations is to demonstrate that the symmetry estimated from the resulting matrix of the STFT applied to a modulated signal can be used to effectively distinguish between two sets of classes (Fig. 7, Fig. 8 and Fig. 9). The first set is composed of signals characterized by low symmetry: LFM signals and polyphase signals (Frank, P1, P2, P3, and P4). The second set is composed of signals which exhibit high symmetry: polytime signals (T1, T2, T3 and T4) and Barker signals. The best surface of separation of these two classes is represented by a red line at Figures 7 to 9. The red line position is the symmetry threshold that minimizes the quantity of incorrect classifications. A different threshold was calculated for each of the following methods of symmetry estimation. Three approaches to template matching, previously unused for estimating symmetry in the time-frequency domain, were compared against the WiSARD proposed method: NCC [35](Eq. (15)), NSAD [34] (Eq. (16)) and NSSD [36](Eq. (17)). The NSAD and NSSD are measures of differences. The greater the similarity between templates, the lower the measured values. For this reason, a negative sign was introduced to estimate the similarity: -NSAD and -NSSD. The results of these simulations are analyzed using a box plot. At Figures 7 and 8, each column represent the symmetry of one specific modulation type.

The NCC, NSAD and NSSD symmetry is estimated as follows. First the STFT is applied to the signal. A bounding box of the region were the signal is present segments the points of interest in the time-frequency plane. A horizontal line passing through the center of the bounding box divides the segmented region into two rectangles, defining the two templates (Fig. 4 and Fig. 5). If the response to the STFT exhibits symmetry, the horizontal line acts as a mirror, meaning that the template below the line is a reflected image of the template above the line. So these three template matching algorithms are measured using two templates, one is the image above the horizontal line and the other is the image under the horizontal line rotated by 180^o.

$$NCC = \sum_{x,y \in T_1 \wedge x,y' \in T_2} \frac{T_1(x,y)T_2(x,y')}{\sqrt{\sum (T_1(x,y))^2}\sqrt{\sum (T_2(x,y'))^2}}, \tag{15}$$

where T_1 is the template 1, T_2 is the template 2, x is the column of a point in T_1, y is the row of a point in T_1, y' is the row of a point in T_2, (x,y) and (x,y') are points equidistant from the horizontal line (Fig. 5).

$$NSAD = \sum_{x,y \in T_1 \wedge x,y' \in T_2} \frac{|T_1(x,y) - T_2(x,y')|}{MAX\,(T_1(x,y) \wedge T_2(x,y'))}, \tag{16}$$

https://doi.org/10.21528/lnlm-vol23-no1-art2

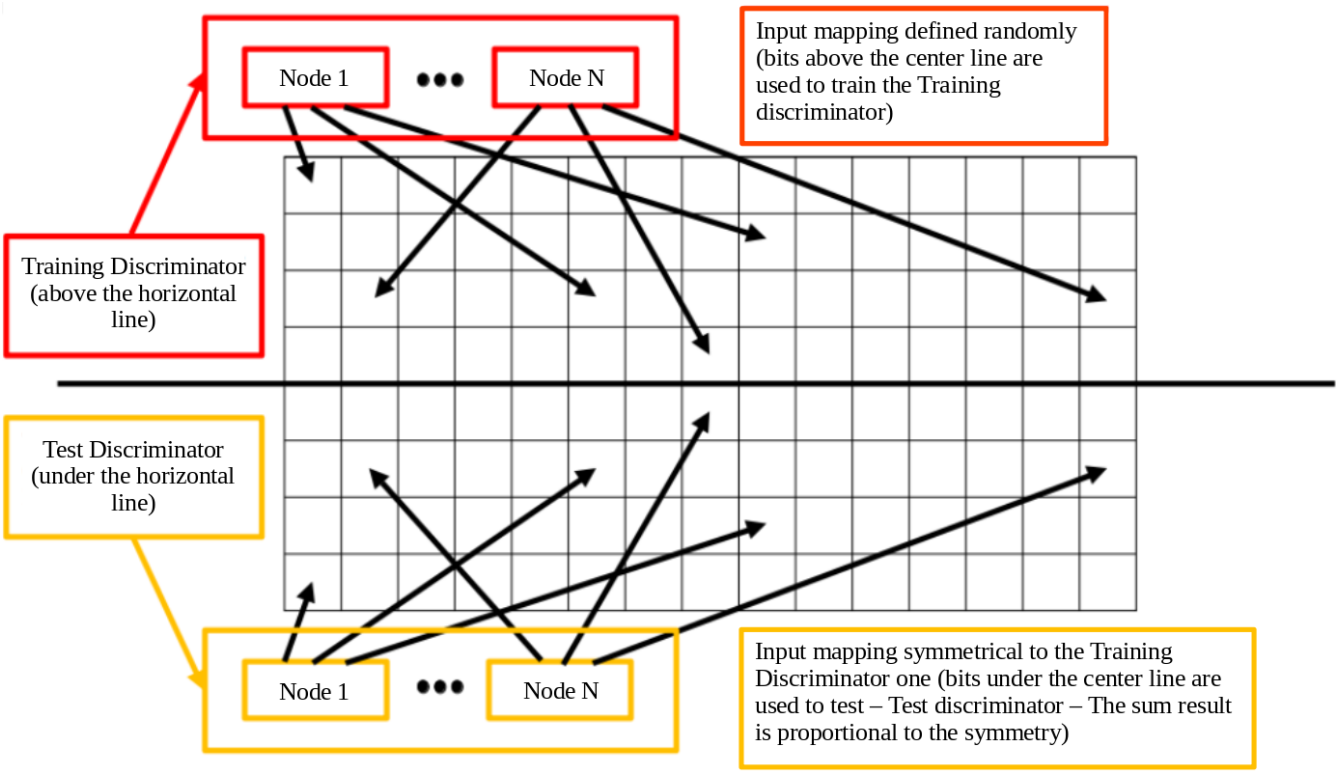

Figure 5: Input mapping of the training discriminators is mirrored to the test discriminator's input mapping. This way the symmetry can be estimated.

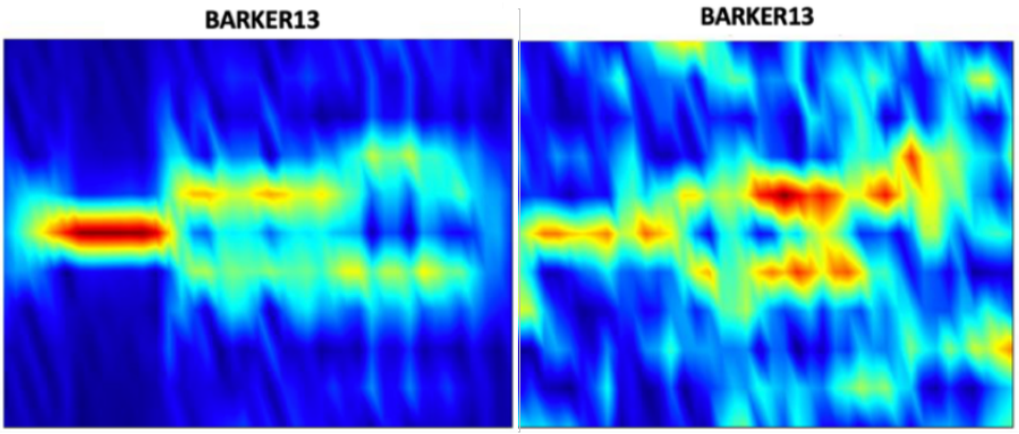

Figure 6: STFT response of a radar signal with Barker signal modulation. On the left there is a signal with SNR = 15dB. On the right there is a signal with SNR = -15dB.

https://doi.org/10.21528/lnlm-vol23-no1-art2

where MAX is the maximum operator.

$$NSSD = \sum_{x,y \in T_1 \wedge x,y' \in T_2} \frac{\left(T_1(x,y) - T_2(x,y')\right)^2}{MAX\left(T_1(x,y) \wedge T_2(x,y')\right)} \tag{17}$$

The first simulation was conducted to demonstrate that the symmetry measure can effectively distinguish between the two sets of signals modulated with $0dB \leq SNR \leq 15dB$ without errors, regardless of the method used to measure symmetry (Fig. 7).

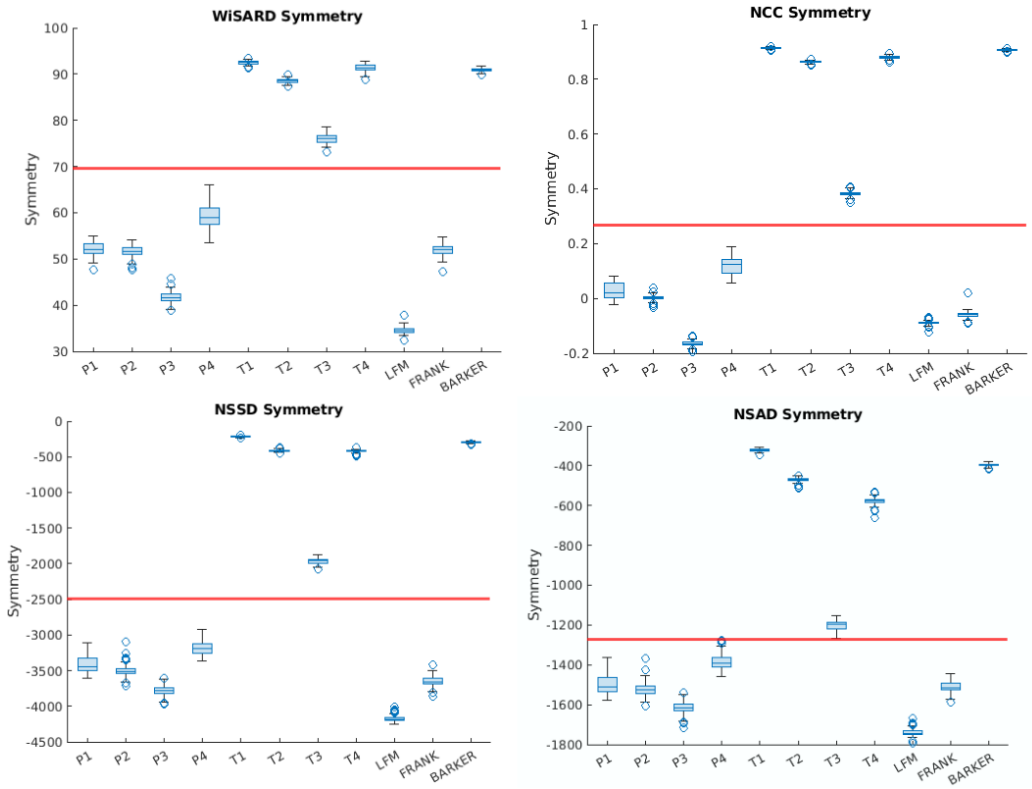

Figure 7: Symmetry estimated using NCC, NSAD, NSSD, and WiSARD for signals modulated with $0dB \leq SNR \leq 15dB$.

The second simulation was conducted to demonstrate that depending on how the symmetry measure is performed, it influences the ability to distinguish between the two sets of modulated signals when signals with low SNR are tested (Fig. 8). In this simulation, signals with $-20dB \leq SNR \leq -10dB$ were used.

Using the accuracy as a form of comparison, the proposed method was the most efficient, producing only 10 incorrect classifications, followed by NCC which produced 20. The NSSD and NSAD methods produced 72 and 111 incorrect classifications respectively. The NSAD on this simulation was the worst estimation method. By using the red line for visual comparison as a separation boundary between the two classes (Fig. 8), the symmetry estimation obtained with NSAD incorrectly classifies most of the T3 modulated signals as belonging to the class of signals without symmetry. In the case of the estimate obtained with NSSD, the separation line between the classes touches the interquartile range of the T3 modulated signals box. The symmetry estimated by the WiSARD network and NCC does not intersect the interquartile range of any of the modulated signal types boxes.

The third simulation has the same objective as the second: to compare the performance of symmetry estimates when the SNR is low (Fig. 9). In this simulation, signals with the lowest SNR were analyzed: $-25dB \leq SNR \leq -20dB$.

Using the accuracy as a form of comparison, the proposed method was the most efficient, producing only 29 incorrect classifications, followed by NCC which produced 37. The NSSD and NSAD methods produced 65 and 89 incorrect classifications respectively. The NSAD on this simulation was the worst estimation method. The symmetry estimation obtained with NSSD and NSAD incorrectly classifies most of T3 modulated signals as belonging to the class of signals without symmetry. The symmetry obtained with NCC is slightly worse than the WiSARD one.

The fourth simulation was conducted to test whether the estimation of symmetry in the time-frequency plane improves the performance of a classifier. For this test, the classifier proposed by Ming [38] was chosen because it is a simple and easily implementable classifier. The classifier consists of two Elman recursive neural networks. The first network separates the input signals into four classes: LFM, Costas, Binary Phase, Polyphase. The second network is responsible for classifying the Polyphase signals into P1, P2, P3, P4, and Frank.

https://doi.org/10.21528/lnlm-vol23-no1-art2

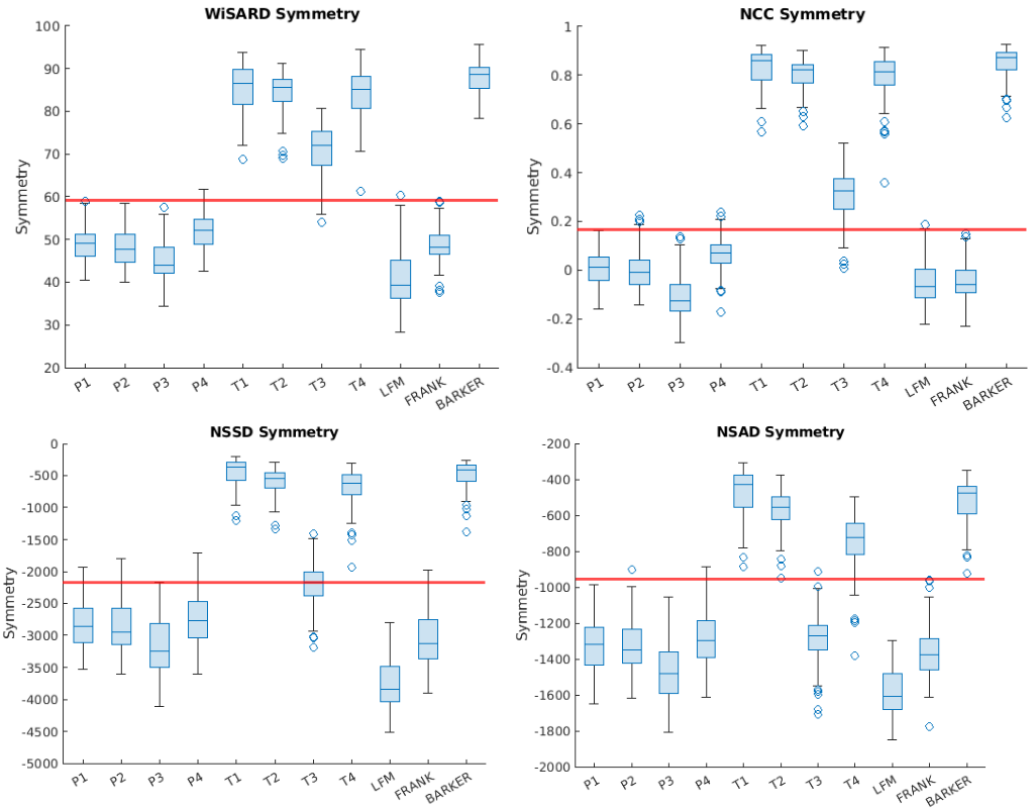

Figure 8: Symmetry estimated using NCC, NSAD, NSSD, and WiSARD for signals modulated with $-20dB \leq SNR \leq -10dB$.

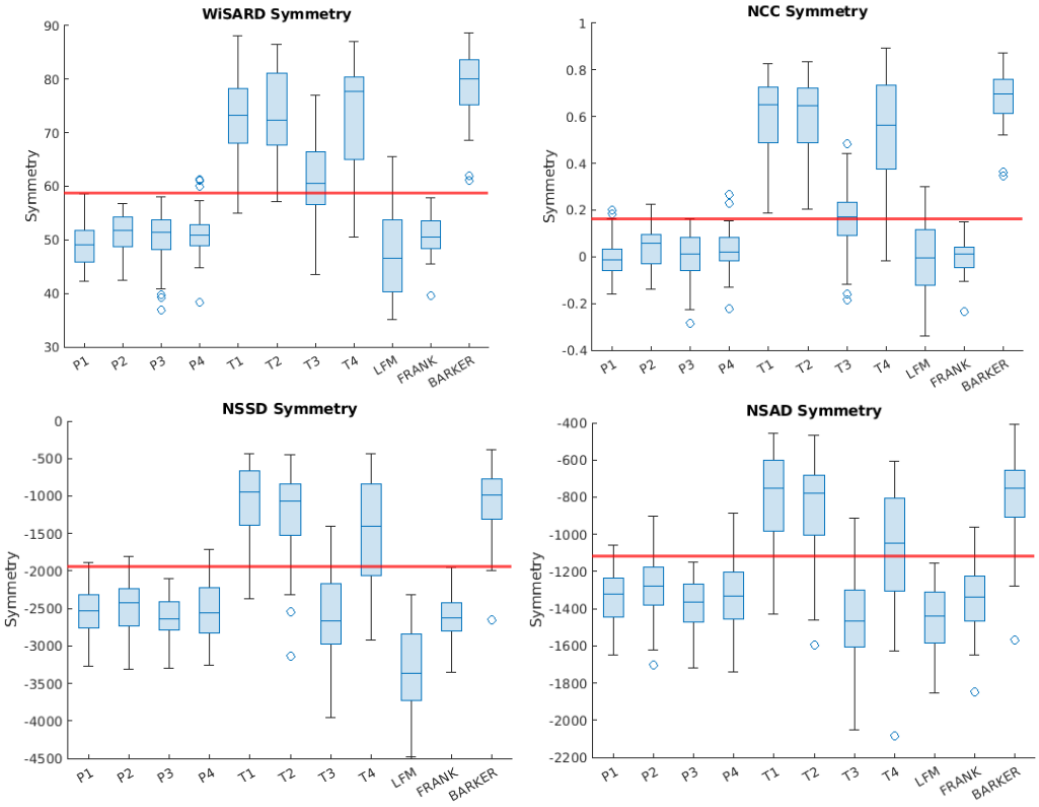

Figure 9: Symmetry estimated using NCC, NSAD, NSSD, and WiSARD for signals modulated with $-25dB \leq SNR \leq -20dB$.

https://doi.org/10.21528/lnlm-vol23-no1-art2

Only the first network of Ming's proposed classifier was used in this simulation. Radar signals from four classes LFM, Pulsed, Barker, and POLY (Polyphase P1, P2, P3, P4, and Frank + Polytime T1, T2, T3, and T4) were used, which the first network should classify. Barker and Polytime classes have high symmetry in the time-frequency plane, while the other classes do not have high symmetry. The first network uses 11 features for classification, some extracted in the time-frequency plane and others extracted in the time domain [38]: Moment M10, Moment M20, Cumulant C20, PSD maximum 1, PSD maximum 2, Standard deviation of instantaneous phase, Standard deviation of instantaneous frequency, Number of objects (10%), Number of objects (50%), CWD time peak location, Standard deviation of object width. The pulse width of the signals is 10 microseconds, and the tested SNRs were: 15dB, 10dB, 5dB, 2.5dB, 0dB, -2.5dB, -5dB, -7.5dB, -10dB, -12.5dB, -15dB, -17.5dB, -20dB, -25dB.

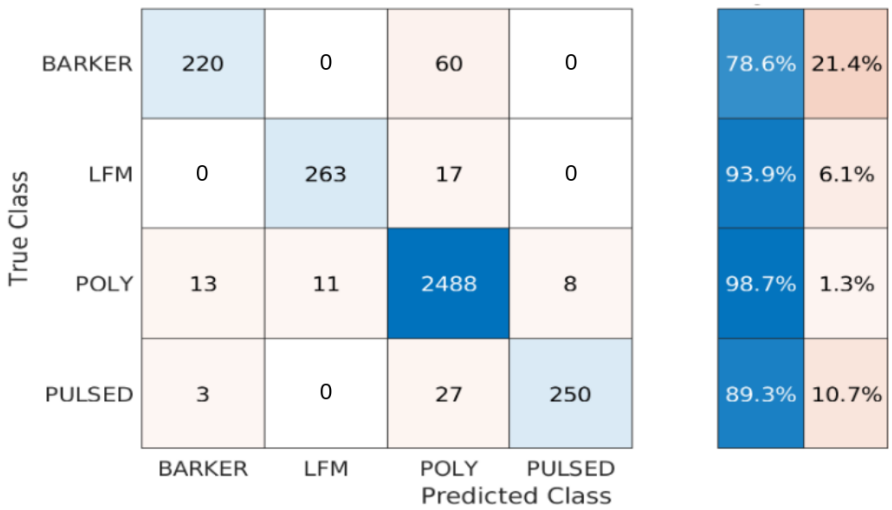

Figure 10: Confusion Matrix obtained from the classification without using symmetry estimation.

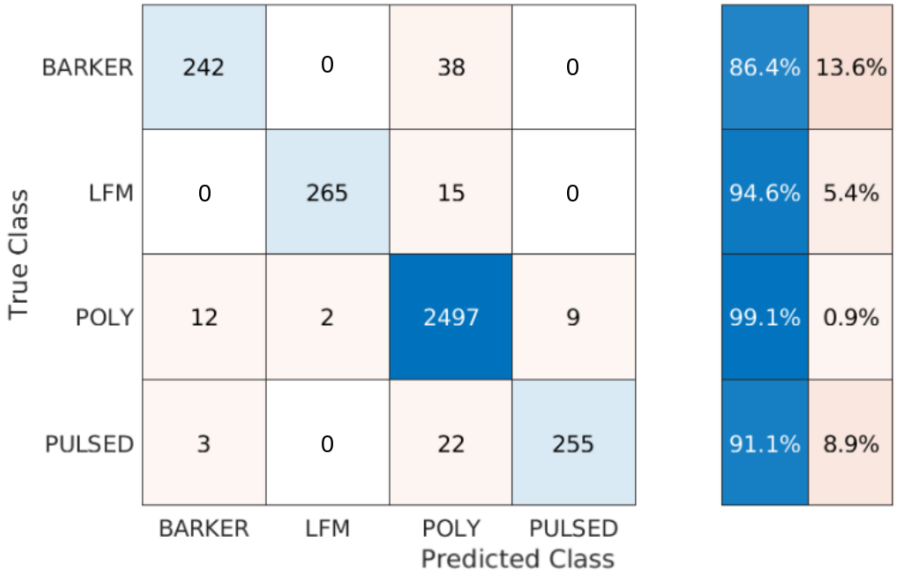

Figure 11: Confusion Matrix obtained from the classification using the symmetry estimated by the WiSARD neural network.

The confusion matrix is a matrix in which the values represent quantities of classifications generated. The rows represent the true classes and the columns represent the classes obtained by the classifier under test. For example, if a class 1 signal is classified as a class 3 signal, 1 is added to the value in line 1 and column 3. The larger the values on the diagonal, the greater the classification accuracy. The accuracy rate of signals from each class, represented with a blue color column, increases with the inclusion of the twentieth feature, the symmetry estimation, especially for signals from the Barker class (Fig. 10 and Fig. 11).

The fifth simulation aims to observe that the lower the SNR, the greater the influence of symmetry estimation on the classifier's performance.

By using signals with SNR $\leq$ -10dB, the accuracy rate increased for all classes, specially the Barker class, that increased from 58% (Fig. 12) to 76% (Fig. 13) with the use of symmetry estimated by the WiSARD network. This increase (from 58%

https://doi.org/10.21528/lnlm-vol23-no1-art2

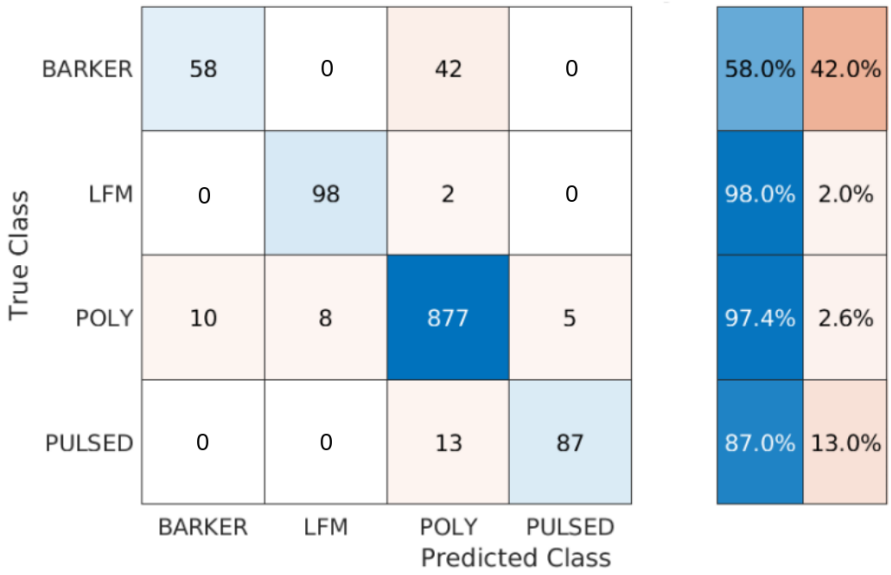

Figure 12: Confusion Matrix obtained from the classification without using symmetry estimation. Only signals with $SNR \leq -10dB$ were considered.

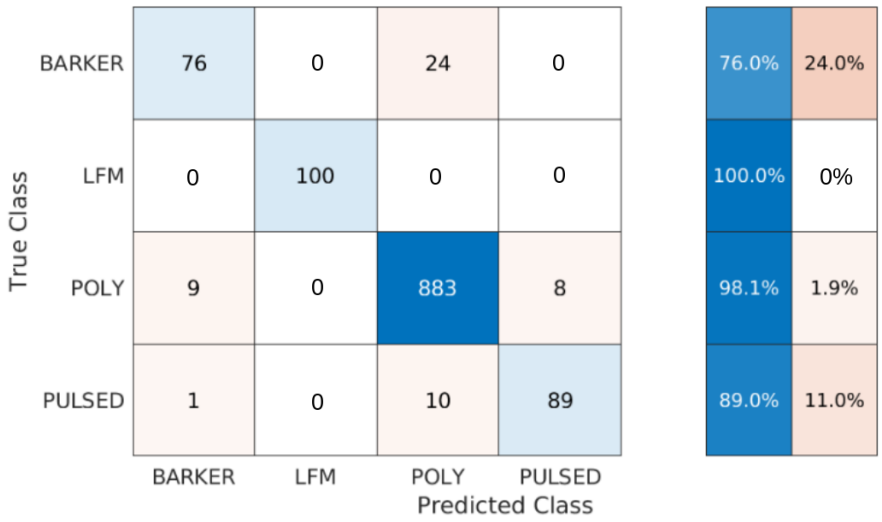

Figure 13: Confusion Matrix obtained from the classification using symmetry estimated by the WiSARD neural network. Only signals with $SNR \leq -10dB$ were considered.

https://doi.org/10.21528/lnlm-vol23-no1-art2

to 76%) was greater than the increase observed with signals at all simulated SNRs (from 78.6% to 86.4%), indicating that the performance improvement is more significant when the SNR is lower.

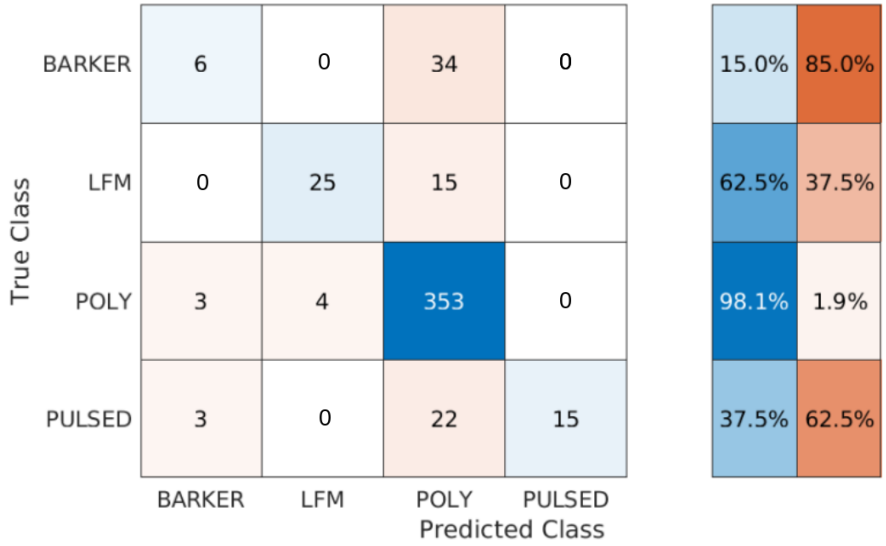

Figure 14: Confusion Matrix obtained from the classification without utilizing symmetry estimation. Only signals with $SNR = -20dB and -25dB$ were considered.

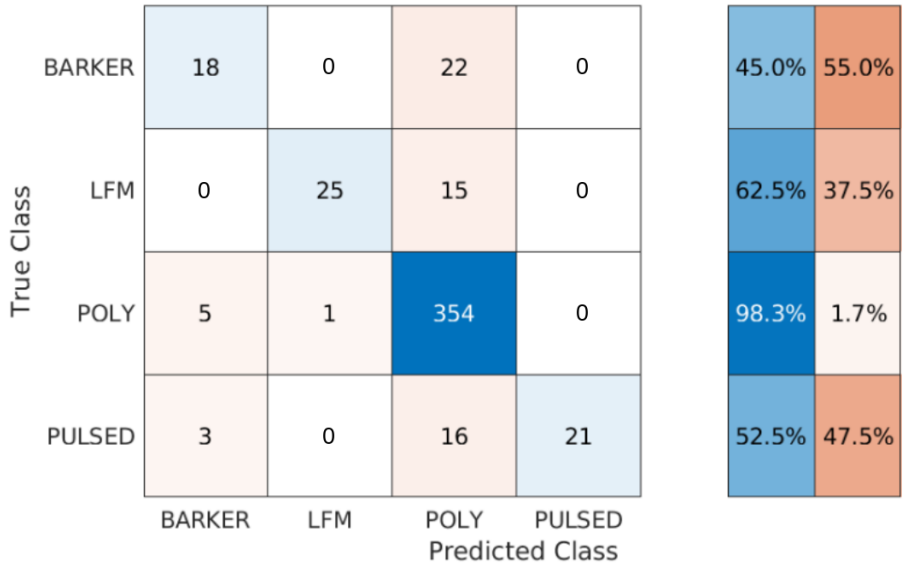

Figure 15: Confusion Matrix obtained from the classification using symmetry estimation by the WiSARD neural network. Only signals with $SNR = -20dB and -25dB$ were considered.

By using signals with SNR = -20dB and -25dB, the accuracy rate of the Barker class, that increased from 15% (Fig. 14) to 45% (Fig. 15) with the use of symmetry estimated by the WiSARD network. This increase (from 15% to 45%) was even greater than the increase observed with signals at SNR $\leq$ -10dB (from 58% to 76%), reinforcing the conclusion that performance improvement is more significant when the SNR is lower.

6. CONCLUSION

The WiSARD neural network is an excellent tool for pattern recognition. It is a simple and fast network. Keeping these characteristics in mind, one of the proposals of this article was to use the WiSARD neural network as a tool to estimate the symmetry present in a phase or frequency-modulated radar signal in the time-frequency plane. The simulations 1 to 3, conducted in section 5, with the aid of the box plot tool, demonstrated that the symmetry estimated by the WiSARD network was more accurate than those estimated using the NCC, NSAD and NSSD measures. These measures are well-known template-matching

measures present in the literature. The WiSARD network was slightly more efficient than the NCC measure, another well-known template matching tool.

The second proposal of this paper, the use of radar pulse symmetry estimation measured on a Time-Frequency (TF) matrix to improve modulation classification was demonstrated through the simulations 4 and 5, conducted in section 5. It was shown that the symmetry estimate extracted from the time-frequency plane can be used as an input feature for a classifier to enhance its performance. The simulations also revealed that the use of symmetry feature estimated from the STFT matrix improves the accuracy of the classifier under all SNR conditions.

For future work, the impact of using time-frequency plane symmetry could be verified using other types of classifiers, and other template-matching measures can be compared with the symmetry extracted with the proposed WiSARD network.

REFERENCES

[1] I. Aleksander, W. V. Thomas and P. A. Bowden. "WiSARD: a radical step forward in image recognition". *Sensor Review*, vol. 4, no. 3, pp. 120–124, 1984.

[2] K. de Aguiar, F. M. G. Franca, V. C. Barbosa and C. A. D. Teixeira. "Early detection of epilepsy seizures based on a weightless neural network". In *2015 37th Annual International Conference of the IEEE Engineering in Medicine and Biology Society (EMBC)*, pp. 4470–4474. IEEE, 2015.

[3] R. D. Cavalcanti, P. M. V. Lima, M. D. Gregorio and D. S. Menasche. "Evaluating weightless neural networks for bias identification on news". In *2017 IEEE 14th International Conference on Networking, Sensing and Control (ICNSC)*, pp. 257–262. IEEE, 2017.

[4] M. D. Gregorio and M. Giordano. "An experimental evaluation of weightless neural networks for multi-class classification". *Applied Soft Computing*, vol. 72, pp. 338–354, 2018.

[5] F. Rangel, F. Firmino, P. M. V. Lima and J. Oliveira. "Semi-Supervised Classification of Social Textual Data Using WiSARD". In *ESANN 2016 proceedings, European Symposium on Artificial Neural Networks, Computational Intelligence and Machine Learning*, pp. 165–170. i6doc.com, 2016.

[6] R. D. S. Moreira and N. F. F. Ebecken. "GWVT: A GPU maritime vessel tracker based on the Wisard Weightless Neural Network". In *2017 Computting Conference*, pp. 738–743. IEEE, 2017.

[7] I. D. S. Miranda *et al.*. "LogicWiSARD: Memoryless Synthesis of Weightless Neural Networks". In *2022 IEEE 33rd International Conference on Application-specific Systems, Architectures and Processors (ASAP)*, pp. 19–26. IEEE Computer Society, 2022.

[8] Q. Guo, X. Yu and G. Rua. "LPI Radar Waveform Recognition Based on Deep Convolutional Neural Network Transfer Learning". *Symmetry*, vol. 11, no. 4, pp. 716–721, 2019.

[9] L. M. Hoang, M. Kim and S.-H. Kong. "Automatic Recognition of General LPI Radar Waveform Using SSD and Supplementary Classifier". *IEEE Transactions on Signal Processing*, vol. 67, no. 13, pp. 3516–3530, 2019.

[10] G. Ghadimi, Y. Norouzi *et al.*. "Deep Learning-Based Approach for Low Probability of Intercept Radar Signal Detection and Classification". *Journal of Communications Technology and Electronics*, vol. 65, no. 10, pp. 1179–1191, 2020.

[11] A. Bektaş and H. Ergezer. "LPI Radar Waveform Classification Using Binary SVM And Multi-Class SVM Based On Principal Components Of Tfi". *Communications Faculty of Sciences University of Ankara Series A2-A3 Physical Sciences and Engineering*, vol. 62, no. 2, pp. 134—-152, 2020.

[12] J. Wan, X. Yu and Q. Guo. "LPI Radar Waveform Recognition Based on CNN and TPOT". *Symmetry*, vol. 11, no. 5, pp. 725, 2019.

[13] Z. Qu, X. Mao and Z. Deng. "Radar Signal Intra-Pulse Modulation Recognition Based on Convolutional Neural Network". *IEEE Access*, vol. 6, pp. 43874–43884, 2018.

[14] D. Quan, Z. Tang *et al.*. "LPI Radar Signal Recognition Based on Dual-Channel CNN and Feature Fusion". *Symmetry*, vol. 14, no. 3, pp. 570, 2022.

[15] C. Yang, Z. Xiong, Y. Guo and B. Zhang. "LPI radar signal detection based on the combination of FFT and segmented autocorrelation plus PAHT". *Journal of Systems Engineering and Electronics*, vol. 28, no. 5, pp. 890–899, 2017.

[16] G. Vanhoy, T. Schucker and T. Bose. "Classification of LPI radar signals using spectral correlation and support vector machines". In *Analog Integr Circuits Signal Process*, pp. 305–313. Springer, 2016.

[17] R. K. Chilukuri, H. K. Kakarla and K. Subbarao. "Estimation of Modulation Parameters of LPI Radar Using Cyclostationary Method". *Sensing and Imaging*, vol. 21, no. 51, pp. 1–20, 2020.

[18] T. R. Kishore and K. D. Rao. "Automatic Intrapulse Modulation Classification of Advanced LPI Radar Waveforms". *IEEE Transactions on Aerospace and Electronic Systems*, vol. 53, no. 2, pp. 901–914, 2017.

[19] R. Barker. "Group synchronizing of binary digital systems". In *Communication theory*, pp. 273–287. American Mathematical Society, 1953.

[20] J. E. Fielding. "Polytime coding as a means of pulse compression". *IEEE Transactions on Aerospace and Electronic Systems*, vol. 35, no. 2, pp. 716–721, 1999.

[21] R. Frank. "Polyphase codes with good nonperiodic correlation properties". *IEEE Transactions on Information Theory*, vol. 9, no. 1, pp. 43–45, 1963.

[22] B. L. Lewis and F. F. Kretschmer. "A New Class of Polyphase Pulse Compression Codes and Techniques". *IEEE Transactions on Aerospace and Electronic Systems*, vol. AES-17, no. 3, pp. 364–372, 1981.

[23] B. L. Lewis and F. F. Kretschmer. "Linear Frequency Modulation Derived Polyphase Pulse Compression Codes". *IEEE Transactions on Aerospace and Electronic Systems*, vol. AES-18, no. 5, pp. 637–641, 1982.

[24] J. R. Klauder, A. C. Price, S. Darlington and W. J. Albersheim. "The theory and design of chirp radars". *The Bell System Technical Journal*, vol. 39, no. 4, pp. 745–808, 1960.

[25] P. Pace. *Detecting and Classifying Low Probability of Intercept Radar*. Artech House Publishers, London, 2008.

[26] A. D. O. P. Silva, J. Costa and R. Moreira. "Application of a Channelized Energy Detector for Digital Wideband ESM Receivers". In *XLI Brazilian symposium on telecommunications and signal processing*, 2023.

[27] S. H. Kong, M. Kim, L. M. Hoang and E. Kim. "Automatic LPI Radar Waveform Recognition Using CNN". *IEEE Access*, vol. 6, pp. 4207–4219, 2018.

[28] Z. Ma, Z. Huang, A. Lin and G. Huang. "LPI Radar Waveform Recognition Based on Features from Multiple Images". *Sensors*, vol. 20, no. 2, 2020.

[29] D. F. P. de Souza, F. M. G. Franca and P. M. V. Lima. "Spatio-temporal Pattern Classification with KernelCanvas and WiSARD". In *2014 Brazilian Conference on Intelligent Systems*, pp. 228–233. IEEE Computer Society, 2014.

[30] T. Chuntama, P. Techa-Angkoon *et al.*. "Multiclass Classification of Astronomical Objects in the Galaxy M81 using Machine Learning Techniques". In *2020 24th International Computer Science and Engineering Conference (ICSEC)*, pp. 1–6. IEEE Computer Society, 2020.

[31] S. Milhomem, T. S. D. Almeida *et al.*. "Weightless Neural Network with Transfer Learning to Detect Distress in Asphalt". *International Journal of Advanced Engineering Research and Science (IJAERS)*, vol. 5, no. 12, pp. 294–299, 2018.

[32] M. D. Gregorio, A. D. Costanzo *et al.*. "Classification of preclinical markers in Alzheimer's disease via WiSARD classifier". In *ESANN 2022 proceedings, European Symposium on Artificial Neural Networks, Computational Intelligence and Machine Learning*, pp. 43–48. i6doc.com, 2022.

[33] L. A. D. L. Filho, F. M. G. Franca and P. M. V. Lima. "Near-optimal facial emotion classification using a WiSARD-based weightless system". In *ESANN 2018 proceedings, European Symposium on Artificial Neural Networks, Computational Intelligence and Machine Learning*, pp. 85–90. i6doc.com, 2018.

[34] J. Cai, P. Huang and D. Wang. "Novel dynamic template matching of visual servoing for tethered space robot". In *IEEE International Conference on Information Science and Technology*, pp. 389–392. IEEE, 2014.

[35] J. N. Sarvaiya, S. Patnaik and S. Bombaywala. "Image Registration by Template Matching Using Normalized Cross-Correlation". In *2009 International Conference on Advances in Computing, Control, and Telecommunication Technologies*, pp. 819–822. IEEE, 2009.

[36] S. Nikan and M. Ahmadi. "Partial Face Recognition Based on Template Matching". In *11th International Conference on Signal-Image Technology and Internet-Based Systems (SITIS)*, pp. 160–163. IEEE, 2015.

[37] I. Aleksander. "Ideal neurons for neural computers". In *International Conference on. Parallel Processing in Neural Systems and Computers*, pp. 225–228. Elsevier Science Publishers, 1990.

[38] M. Zhang, L. Liu and M. Diao. "LPI Radar Waveform Recognition Based on Time-Frequency Distribution". *Sensors*, vol. 16, no. 10, pp. 1–20, 2016.